

# JANOSSY POOLING: LEARNING DEEP PERMUTATION-INVARIANT FUNCTIONS FOR VARIABLE-SIZE INPUTS

**Ryan L. Murphy**

Department of Statistics  
Purdue University  
murph213@purdue.edu

**Balasubramaniam Srinivasan**

Department of Computer Science  
Purdue University  
bsriniv@purdue.edu

**Vinayak Rao**

Department of Statistics  
Purdue University  
varao@purdue.edu

**Bruno Ribeiro**

Department of Computer Science  
Purdue University  
ribeiro@cs.purdue.edu

## ABSTRACT

We consider a simple and overarching representation for permutation-invariant functions of sequences (or set functions). Our approach, which we call Janossy pooling, expresses a permutation-invariant function as the average of a permutation-sensitive function applied to all reorderings of the input sequence. This allows us to leverage the rich and mature literature on permutation-sensitive functions to construct novel and flexible permutation-invariant functions. If carried out naively, Janossy pooling can be computationally prohibitive. To allow computational tractability, we consider three kinds of approximations: canonical orderings of sequences, functions with  $k$ -order interactions, and stochastic optimization algorithms with random permutations. Our framework unifies a variety of existing work in the literature, and suggests possible modeling and algorithmic extensions. We explore a few in our experiments, which demonstrate improved performance over current state-of-the-art methods.

## 1 INTRODUCTION

Pooling is a fundamental operation in deep learning architectures (LeCun et al., 2015). The role of pooling is to merge a collection of related features into a single, possibly vector-valued, summary feature. A prototypical example is in convolutional neural networks (CNNs) (LeCun et al., 1995), where linear activations of features in neighborhoods of image locations are pooled together to construct more abstract features. A more modern example is in neural networks for graphs, where each layer pools together embeddings of neighbors of a vertex to form a new embedding for that vertex, see for instance, (Kipf & Welling, 2016; Atwood & Towsley, 2016; Hamilton et al., 2017; Velickovic et al., 2017; Monti et al., 2017; Xu et al., 2018; Liu et al., 2018; Liben-Nowell & Kleinberg, 2007; van den Berg et al., 2017; Duvenaud et al., 2015; Gilmer et al., 2017; Ying et al., 2018).

A common requirement of a pooling operator is invariance to the ordering of the input features. In CNNs for images, this allows invariance to translations and rotations of objects, while for graphs, this allows invariance to relabeling of graph vertices. Existing pooling operators are mostly limited to pre-defined heuristics such as max-pool, min-pool, sum, or average. Another desirable characteristic of pooling layers is the ability to take variable-size inputs. This is less important in images, where neighborhoods are usually fixed *a priori*. However in applications involving graphs, the number of neighbors of different vertices can vary widely. Our goal is to design flexible and learnable pooling operators satisfying these two desiderata.

Abstractly, we will view pooling as a permutation-invariant (or symmetric) function acting on finite but arbitrary length sequences  $\mathbf{h}$ . All elements  $h_i$  of the sequences are features lying in some space  $\mathbb{H}$  (which itself could be a high-dimensional Euclidean space  $\mathbb{R}^d$  or some subset thereof). The sequences  $\mathbf{h}$  are themselves elements of the union of products of the  $\mathbb{H}$ -space:  $\mathbf{h} \in \bigcup_{j=0}^{\infty} \mathbb{H}^j \equiv \mathbb{H}^{\cup}$ . Throughout the paper, we will use  $\Pi_n$  to represent the set of all permutations of the integers 1 to  $n$ ,

where  $n$  will often be clear from the context. In addition,  $\mathbf{h}_\pi$ ,  $\pi \in \Pi_{|\mathbf{h}|}$ , will represent a reordering of the elements of a sequence  $\mathbf{h}$  according to  $\pi$ , where  $|\mathbf{h}|$  is the length of the sequence  $\mathbf{h}$ . We will use the double bar superscript  $\overline{\overline{f}}$  to indicate that a function is permutation-invariant, returning the same value no matter the order of its arguments:  $\overline{\overline{f}}(\mathbf{h}) = \overline{\overline{f}}(\mathbf{h}_\pi)$ ,  $\forall \pi \in \Pi_{|\mathbf{h}|}$ . We will use the arrow superscript  $\overrightarrow{f}$  to indicate general functions on sequences  $\mathbf{h}$  which may or may not be permutation-invariant. Functions  $f$  without any markers are ‘simple’ functions, acting on elements in  $\mathbb{H}$ , scalars or any other argument that is not a sequence of elements in  $\mathbb{H}$ .

Our goal in this paper is to model and learn permutation-sensitive functions  $\overrightarrow{f}$  that can be used to construct flexible and learnable permutation-invariant neural networks. A recent step in this direction is work on *deep sets* by Zaheer et al. (2017), who argued for learning permutation-invariant functions through the following composition:

$$\overline{\overline{y}}(\mathbf{x}; \boldsymbol{\theta}^{(\rho)}, \boldsymbol{\theta}^{(f)}, \boldsymbol{\theta}^{(h)}) = \rho\left(\overline{\overline{f}}(|\mathbf{h}|, \mathbf{h}; \boldsymbol{\theta}^{(f)}); \boldsymbol{\theta}^{(\rho)}\right), \text{ where} \quad (1)$$

$$\overline{\overline{f}}(|\mathbf{h}|, \mathbf{h}; \boldsymbol{\theta}^{(f)}) = \sum_{j=1}^{|\mathbf{h}|} f(h_j; \boldsymbol{\theta}^{(f)}) \quad \text{and} \quad \mathbf{h} \equiv h(\mathbf{x}; \boldsymbol{\theta}^{(h)}). \quad (2)$$

Here (a)  $\mathbf{x} \in \mathbb{X}$  is one observation in the training data,  $\mathbf{h} \in \mathbb{H}$  is the embedding (output) of the data given by the lower layers  $h : \mathbb{X} \times \mathbb{R}^a \rightarrow \mathbb{H}^U$ ,  $a > 0$  with parameters  $\boldsymbol{\theta}^{(h)} \in \mathbb{R}^a$ ; (b)  $f : \mathbb{H} \times \mathbb{R}^b \rightarrow \mathbb{F}$  is a middle-layer embedding function with parameters  $\boldsymbol{\theta}^{(f)} \in \mathbb{R}^b$ ,  $b > 0$ , and  $\mathbb{F}$  is the embedding space of  $f$ ; and (c)  $\rho : \mathbb{F} \times \mathbb{R}^c \rightarrow \mathbb{Y}$  is a neural network with parameters  $\boldsymbol{\theta}^{(\rho)} \in \mathbb{R}^c$ ,  $c > 0$ , that maps to the final output space  $\mathbb{Y}$ . Typically  $\mathbb{H}$  and  $\mathbb{F}$  are high-dimensional real-valued spaces;  $\mathbb{Y}$  is often  $\mathbb{R}^d$  in  $d$ -dimensional regression problems or the simplex in classification problems. Effectively, the neural network  $f$  learns an embedding for each element in  $\mathbb{H}$ , and given a sequence  $\mathbf{h}$ , its component embeddings are added together before a second neural network transformation  $\rho$  is applied. Note that the function  $h$  may be the identity mapping  $h(\mathbf{x}; \cdot) = \mathbf{x}$  that makes  $\overline{\overline{f}}$  act directly on the input data. Zaheer et al. (2017) argues that, under reasonable assumptions, the above architecture with suitably flexible functions  $f$  and  $\rho$  is capable of approximating any symmetric function on  $\mathbf{h}$ -sequences, which justifies the widespread use of average (sum) pooling to make neural networks permutation-invariant in Duvenaud et al. (2015), Hamilton et al. (2017), Kipf & Welling (2016), Atwood & Towsley (2016), among other works.

In practice, however, there is a gap between flexibility and learnability. While the architecture of equations 1 and 2 is a universal approximator to all permutation-invariant functions, it does not allow structural knowledge about the function  $\overline{\overline{y}}$  to be encoded easily. Consider for instance trying to learn the permutation-invariant function  $\overline{\overline{y}}(\mathbf{x}) = \max_{i,j \leq |\mathbf{x}|} |x_i - x_j|$ . With such higher-order interactions between the elements of  $\mathbf{h}$ , the functions  $f$  of equation 2 cannot capture any useful intermediate representations towards the final output, with the burden shifted entirely to the function  $\rho$ . Learning  $\rho$  means learning to undo mixing performed by the summation layer  $\overline{\overline{f}}(|\mathbf{h}|, \mathbf{h}; \boldsymbol{\theta}^{(f)}) = \sum_{j=1}^{|\mathbf{h}|} f(h_j; \boldsymbol{\theta}^{(f)})$ . Unfortunately, as we show in our experiments, in many applications this is too much to ask of  $\rho$ .

**Contributions.** In this work we investigate a learnable permutation-invariant pooling layer for variable-size inputs inspired by the Janossy density framework (widely used in the theory of point processes (Daley & Vere-Jones, 2003, Chapter 7)). This approach, which we call Janossy

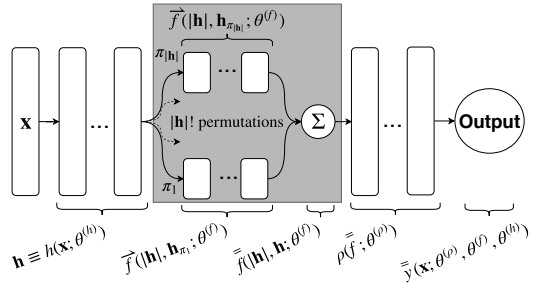


Figure 1: A neural network with a single Janossy pooling layer. The embedding  $\mathbf{h}$  is permuted in all  $|\mathbf{h}|!$  possible ways, and for each permutation  $\mathbf{h}_\pi$ ,  $f(|\mathbf{h}|, \mathbf{h}_\pi; \boldsymbol{\theta}^{(f)})$  is computed. These results are added together and the result is passed to a second function  $\rho$  parameterized by  $\boldsymbol{\theta}^{(\rho)}$ , which gives the final permutation-invariant output  $\overline{\overline{y}}(\mathbf{x}; \boldsymbol{\theta}^{(\rho)}, \boldsymbol{\theta}^{(f)}, \boldsymbol{\theta}^{(h)})$ ; the gray rectangle represents Janossy pooling. We discuss how this scheme can be made computationally tractable.

pooling, directly allows the user to model what higher-order dependencies in  $\mathbf{h}$  are relevant in the pooling.

Figure 1 summarizes a neural network with a single pooling layer  $\bar{\bar{f}}$ : given an input embedding  $\mathbf{h}$ , we apply a learnable (permutation-sensitive) function  $\bar{f}$  to every permutation  $\mathbf{h}_\pi$  of the input sequence  $\mathbf{h}$ . These outputs are added together, and fed to the second function  $\rho$ . Examples of function  $\bar{f}$  include feedforward and recurrent neural networks (RNNs). We call the operation used to construct  $\bar{\bar{f}}$  from  $\bar{f}$  the *Janossy pooling*. A more detailed description of Janossy pooling is given in Definition 2.1. Further, we contribute the following analysis:

- (a) We show *deep sets* (Zaheer et al., 2017) is a special case of Janossy pooling if the function  $\bar{f}$  depends only on the first element of the vector  $\mathbf{h}_\pi$ . In the most general form of Janossy pooling (as described above),  $\bar{f}$  depends on its entire input sequence  $\mathbf{h}_\pi$ . This naturally raises the possibility of intermediate choices of  $\bar{f}$  that allow practitioners to trade between flexibility and tractability. We will show that functions  $\bar{f}$  that depend on their first  $k$  arguments of  $\mathbf{h}_\pi$  allow the Janossy pooling layer to capture up to  $k$ -ary dependencies in  $\mathbf{h}$ .
- (b) We show Janossy pooling can be used to learn permutation-invariant neural networks  $\bar{\bar{y}}(\mathbf{x})$  by sampling a random permutation of  $\mathbf{h}$  during training, and then modeling this permuted sequence using a sequence model such as a recurrent neural network (LSTMs (Hochreiter & Schmidhuber, 1997), GRUs (Cho et al., 2014)) or a vector model such as a feedforward network. We call this permutation-sampling learning algorithm  $\pi$ -SGD ( $\pi$ -Stochastic Gradient Descent). Our analysis explains why this seemingly unsound procedure is theoretically justified, which sheds light on the recent puzzling success of permutation sampling and LSTMs in relational models (Moore & Neville, 2017; Hamilton et al., 2017). We show that this property relates to randomized model ensemble techniques.
- (c) In Zaheer et al. (2017), the authors describe a connection between *deep sets* and infinite de Finetti exchangeability. We provide a probabilistic connection between Janossy pooling and *finite* de Finetti exchangeability (Diaconis, 1977).

## 2 JANOSSY POOLING

In this section we formalize the Janossy pooling function  $\bar{\bar{f}}$ . We start with a function  $\bar{f}$ , parameterized by  $\theta^{(f)}$ , which can take any variable-size sequence as input: a sequence of matrices (such as a sequence of images), a sequence of vectors (such as a sequence of vector embeddings), or a variable-size sequence of features or embeddings representing the neighbors of a node in an attributed graph. In practice, we implement  $\bar{f}$  with a neural network. Formalizing Figure 1 from Section 1, we use  $\bar{f}$  to define  $\bar{\bar{f}}$ :

*Definition 2.1:* [Janossy pooling] Consider a function  $\bar{f} : \mathbb{N} \times \mathbb{H}^U \times \mathbb{R}^b \rightarrow \mathbb{F}$  on variable-length but finite sequences  $\mathbf{h}$ , parameterized by  $\theta^{(f)} \in \mathbb{R}^b$ ,  $b > 0$ . A permutation-invariant function  $\bar{\bar{f}} : \mathbb{N} \times \mathbb{H}^U \rightarrow \mathbb{F}$  is the Janossy function associated with  $\bar{f}$  if

$$\bar{\bar{f}}(|\mathbf{h}|, \mathbf{h}; \theta^{(f)}) = \frac{1}{|\mathbf{h}|!} \sum_{\pi \in \Pi_{|\mathbf{h}|}} \bar{f}(|\mathbf{h}|, \mathbf{h}_\pi; \theta^{(f)}), \quad (3)$$

where  $\Pi_{|\mathbf{h}|}$  is the set of all permutations of the integers 1 to  $|\mathbf{h}|$ , and  $\mathbf{h}_\pi$  represents a particular reordering of the elements of sequence  $\mathbf{h}$  according to  $\pi \in \Pi_{|\mathbf{h}|}$ . We refer the operation used to construct  $\bar{\bar{f}}$  from  $\bar{f}$  as Janossy pooling.  $\diamond$

Definition 2.1 provides a conceptually simple approach for constructing permutation-invariant functions from arbitrary and powerful permutation-sensitive functions such as feedforward networks, recurrent neural networks, or convolutional neural networks. If  $\bar{f}$  is a vector-valued function, then so is  $\bar{\bar{f}}$ , and in practice, one might pass this vector output of  $\bar{\bar{f}}$  through a second function  $\rho$  (e.g. a

neural network parameterized by  $\theta^{(\rho)}$ :

$$\bar{y}(\mathbf{x}; \theta^{(\rho)}, \theta^{(f)}, \theta^{(h)}) = \rho \left( \frac{1}{|\mathbf{h}|!} \sum_{\pi \in \Pi_{|\mathbf{h}|}} \bar{f}(|\mathbf{h}|, \mathbf{h}_\pi; \theta^{(f)}); \theta^{(\rho)} \right), \text{ where } \mathbf{h} \equiv h(\mathbf{x}; \theta^{(h)}). \quad (4)$$

Theoretically, equation 3 can capture any permutation-invariant function for a flexible enough family of functions for  $\bar{f}$ , thus, at least theoretically,  $\rho$  in equation 4 provides no additional representational power. In practice,  $\rho$  can improve learnability by capturing common aspects across all terms in the summation. Furthermore, when we look at approximations to equation 3 or restrictions of  $\bar{f}$  to more tractable families, adding  $\rho$  can help recover some of the lost model capacity. Overall then, equation 4 represents one layer of Janossy pooling, forming a constituent part of a bigger neural network. Figure 1 summarizes this.

Janossy pooling, as defined in equation 3 and 4 is intractable; the computational cost of summing over all permutations (for prediction), and backpropagating gradients (for learning) is likely prohibitive for most problems of interest. Nevertheless, it provides an overarching framework to unify existing methods, and to extend them. In what follows we present strategies for mitigating this, allowing novel and effective trade-offs between learnability and computational cost.

## 2.1 TRACTABILITY THROUGH CANONICAL INPUT ORDERINGS

A simple way to achieve permutation-invariance without the summation in equation 3 is to order the elements of  $\mathbf{h}$  according to some canonical ordering based on its values, and then feed the reordered sequence to  $\bar{f}$ . This way, all the permutations of  $\mathbf{h}$  are mapped to the same canonical sequence. Effectively, this imposes the following structural constraint on  $\bar{f}$ :  $\bar{f}(\mathbf{h})$  equals 0 for all sequences that do not follow the canonical permutation. This then allows complex  $\bar{f}$  models, such as LSTMs and GRUs, that can capture arbitrary relationships in the canonical ordering of  $\mathbf{h}$ .

Examples of the canonical ordering approach already exist in the literature, for example, Niepert et al. (2016) order nodes in a graph according to a user-specified ranking such as betweenness centrality (say from high to low). This approach is useful only if the canonical ordering is relevant to the task at hand. Niepert et al. (2016) acknowledges this shortcoming and Moore & Neville (2017) demonstrates that an ordering by Personalized PageRank (Page et al., 1999; Jeh & Widom, 2003) achieves a lower classification accuracy than a random ordering. As an idealized example, consider input sequences  $\mathbf{h} = ((h_{i,1}, h_{i,2}))_{i=1}^n$ , with  $(h_{i,1}, h_{i,2}) \in \mathbb{H} = \mathbb{R}^2$ , and components  $h_{i,1}$  and  $h_{i,2}$  sampled independently of each other. Choosing to sort  $\mathbf{h}$  according to  $h_{\cdot,1}$  when the task at hand depends on sorting according to  $h_{\cdot,2}$  can lead to poor prediction accuracy.

Rather than pre-defining a good canonical order, one can try to learn it from the data. This requires searching over the discrete space of all  $|\mathbf{h}|!$  permutations of the input vector  $\mathbf{h}$ . In practice, this discrete optimization relies on heuristics (Vinyals et al., 2016; Rezatofighi et al., 2018). Alternatively, instead of choosing a single canonical ordering, one can choose multiple orderings, resulting in ensemble methods that average across multiple permutations. These can be viewed as more refined (possibly data-driven) approximations to equation 3.

## 2.2 TRACTABILITY THROUGH $k$ -ARY DEPENDENCIES

Here, we provide a different spectrum of options to trade-off flexibility, complexity, and generalizability in Janossy pooling. Now, to simplify the sum over permutations in equation 3, we impose structural constraints where  $\bar{f}(\mathbf{h})$  depends only on the first  $k$  elements of its input sequence. This amounts to the assumption that only  $k$ -ary dependencies in  $\mathbf{h}$  are relevant to the task at hand.

*Definition 2.2:* [ $k$ -ary Janossy pooling] Fix  $k \in \mathbb{N}$ . For any sequence  $\mathbf{h}$ , define  $\downarrow_k(\mathbf{h})$  as its projection to a length  $k$  sequence; in particular, if  $|\mathbf{h}| \geq k$ , we keep the first  $k$  elements. Then, a  $k$ -ary permutation-invariant Janossy function  $\bar{f}$  is given by

$$\bar{f}(|\mathbf{h}|, \mathbf{h}; \theta^{(f)}) = \frac{1}{|\mathbf{h}|!} \sum_{\pi \in \Pi_{|\mathbf{h}|}} \bar{f}(|\mathbf{h}|, \downarrow_k(\mathbf{h}_\pi); \theta^{(f)}). \quad (5)$$

◇

Note that if some of the embeddings have length  $|\mathbf{h}| < k$ , then we can zero pad to form the length- $k$  sequence  $(\downarrow_k(\mathbf{h}_\pi), 0, \dots, 0)$ .

Proposition 2.1 shows that if  $|\mathbf{h}| > k$ , equation 5 only needs to sum over  $|\mathbf{h}|!/(|\mathbf{h}| - k)!$  terms, which can be tractable for small  $k$ .

**Proposition 2.1.** *The Janossy pooling in equation 5 requires summing over only  $\frac{|\mathbf{h}|!}{(|\mathbf{h}| - k)!}$  terms, thus saving computation when  $k < |\mathbf{h}|$ .*

*Proof.* Define two permutations  $\pi, \pi' \in \Pi_{|\mathbf{h}|}$  that agree on the first  $k$  elements as  $k$ -equivalent. Such permutations satisfy  $\vec{f}(|\mathbf{h}|, \downarrow_k(\mathbf{h}_\pi); \boldsymbol{\theta}^{(f)}) = \vec{f}(|\mathbf{h}|, \downarrow_k(\mathbf{h}_{\pi'}); \boldsymbol{\theta}^{(f)})$ . These two permutations belong to the same equivalence class, containing a total of  $(|\mathbf{h}| - k)!$  permutations (obtained by permuting the last  $(|\mathbf{h}| - k)$  elements). Overall, we then have a total of  $|\mathbf{h}|!/(|\mathbf{h}| - k)!$  equivalence classes. Write the set of equivalence classes as  $\Pi_{|\mathbf{h}|}^k$ , and represent each by one of its elements. Then,

$$\bar{\vec{f}}(|\mathbf{h}|, \mathbf{h}; \boldsymbol{\theta}^{(f)}) = \frac{1}{|\mathbf{h}|!} \sum_{\pi \in \Pi_{|\mathbf{h}|}} \vec{f}(|\mathbf{h}|, \downarrow_k(\mathbf{h}_\pi); \boldsymbol{\theta}^{(f)}) = \frac{(|\mathbf{h}| - k)!}{|\mathbf{h}|!} \sum_{\pi \in \Pi_{|\mathbf{h}|}^k} \vec{f}(|\mathbf{h}|, \downarrow_k(\mathbf{h}_\pi); \boldsymbol{\theta}^{(f)})$$

is now a summation over only  $|\mathbf{h}|!/(|\mathbf{h}| - k)!$  terms. □

The sum in equation 5 can be written equivalently as  $\sum_{i_1, i_2, \dots, i_k \in \mathbb{I}_{|\mathbf{h}|}} \vec{f}(|\mathbf{h}|, \mathbf{h}_{i_1, i_2, \dots, i_k}; \boldsymbol{\theta}^{(f)})$ , where  $\mathbb{I}_{|\mathbf{h}|}$  is the set of all permutations of  $\{1, 2, \dots, |\mathbf{h}|\}$  taken  $k$  at a time. Note that the value of  $k$  balances computational savings and model flexibility; it can be selected as a hyperparameter based on a-priori beliefs or through typical hyperparameter tuning strategies.

**Remark 2.1** (Deep sets (Zaheer et al., 2017) is a 1-ary (unary) Janossy pooling). *Equation 5 represented with  $k = 1$  and composing with  $\rho$  as in equation 4 yields the model  $\rho(\frac{1}{|\mathbf{h}|} \sum_{i=1}^{|\mathbf{h}|} \vec{f}(|\mathbf{h}|, h_i; \boldsymbol{\theta}^{(f)}); \boldsymbol{\theta}^{(\rho)})$  which can be easily seen to yield equation 2 for an appropriate choice of  $\vec{f}$ .*

Not surprisingly, the computational savings obtained from  $k$ -ary Janossy pooling come at the cost of reduced model flexibility. The next result formalizes this.

**Theorem 2.1.** *For any  $k \in \mathbb{N}$ , define  $\mathcal{F}_k$  as the set of all permutation-invariant functions that can be represented by Janossy pooling with  $k$ -ary dependencies. Then,  $\mathcal{F}_{k-1}$  is a proper subset of  $\mathcal{F}_k$  if the space  $\mathbb{H}$  is not trivial (i.e. if the cardinality of  $\mathbb{H}$  is greater than 1). Thus, Janossy pooling with  $k$ -ary dependencies can express any Janossy pooling function with  $(k - 1)$ -ary dependencies, but the converse does not hold.*

*Proof.*

$(\mathcal{F}_{k-1} \subset \mathcal{F}_k)$ : Consider any element  $\bar{\vec{f}}_{k-1} \in \mathcal{F}_{k-1}$ , and write  $\vec{f}(|\mathbf{h}|, \cdot; \boldsymbol{\theta}^{(f)})$  for its associated Janossy function. For any sequence  $\mathbf{h}$ ,  $\vec{f}(|\mathbf{h}|, \downarrow_{k-1}(\mathbf{h}); \boldsymbol{\theta}^{(f)}) = \vec{f}(|\mathbf{h}|, \downarrow_{k-1}(\downarrow_k(\mathbf{h})); \boldsymbol{\theta}^{(f)}) := \vec{f}_+(\mathbf{h}, \downarrow_k(\mathbf{h}); \boldsymbol{\theta}^{(f)})$ , where the function  $\vec{f}_+$  looks at its first  $k$  elements. Thus,

$$\begin{aligned} \bar{\vec{f}}_{k-1}(|\mathbf{h}|, \mathbf{h}; \boldsymbol{\theta}^{(f)}) &= \frac{1}{|\mathbf{h}|!} \sum_{\pi \in \Pi_{|\mathbf{h}|}} \vec{f}(|\mathbf{h}|, \downarrow_{k-1}(\mathbf{h}_\pi); \boldsymbol{\theta}^{(f)}) = \frac{1}{|\mathbf{h}|!} \sum_{\pi \in \Pi_{|\mathbf{h}|}} \vec{f}_+(\mathbf{h}, \downarrow_k(\mathbf{h}_\pi); \boldsymbol{\theta}^{(f)}) \\ &= \bar{\vec{f}}_k(|\mathbf{h}|, \mathbf{h}; \boldsymbol{\theta}^{(f)}), \end{aligned} \tag{6}$$

where  $\bar{\vec{f}}_k$  is the Janossy function associated with  $\vec{f}_+$  and thus belongs to  $\mathcal{F}_k$ .

$(\mathcal{F}_k \not\subset \mathcal{F}_{k-1})$ : Here, we need to construct a function  $\bar{\vec{f}}_k \in \mathcal{F}_k$  that is not present in  $\mathcal{F}_{k-1}$ . The construction is given in the Supplementary Material. □

**Corollary 2.1.** *For  $k > 1$ , the deep sets function in equation 1 (Zaheer et al., 2017) pushes the modeling of  $k$ -ary relationships to  $\rho$ .*

*Proof.* Deep sets functions can be expressed via Janossy pooling with  $k = 1$ . Thus, by Theorem 2.1,  $\bar{\vec{f}}$  in equation 2 cannot express all functions that can be expressed by higher-order (i.e.  $k > 1$ ) Janossy pooling operations. Consequently, if the deep sets function can express any permutation-invariant function, the expressive power must have been pushed to  $\rho$ . □

### 2.3 TRACTABILITY THROUGH PERMUTATION SAMPLING

Another approach to tractable Janossy pooling samples *random* permutations of the input  $\mathbf{h}$  during training. Like the canonical ordering approach of Section 2.1, this offers significant computational savings, allowing more complex models for  $\bar{f}$  such as LSTMs and GRUs. However, in contrast with that approach, this is considerably more flexible, avoiding the need to learn a canonical ordering or to make assumptions about the dependencies between the elements of  $\mathbf{h}$  and the objective function. The approach of sampling random permutations has been previously used in relational learning tasks (Moore & Neville, 2017; Hamilton et al., 2017) as a heuristic with an LSTM as  $\bar{f}$ . Both these papers report that permutation sampling outperforms or closely matches other tested neural network models they tried. We provide a theoretical framework to understand and extend such approaches.

For the sake of simplicity, we analyze the optimization with a single sampled permutation. However, note that increasing the number of sampled permutations in the estimate of  $\bar{f}$  decreases variance, and we recover the exact algorithm when all  $|\mathbf{h}|!$  permutations are sampled. We assume a supervised learning setting, though our analysis easily extends to unsupervised learning. We are given training data  $\mathcal{D} \equiv \{(\mathbf{x}_1, \mathbf{y}_1), \dots, (\mathbf{x}_N, \mathbf{y}_N)\}$ , where  $\mathbf{y}_i \in \mathbb{Y}$  is the target output and  $\mathbf{x}_i$  its corresponding input. Our original goal was to minimize the empirical loss

$$\bar{L}(\mathcal{D}; \boldsymbol{\theta}^{(\rho)}, \boldsymbol{\theta}^{(f)}, \boldsymbol{\theta}^{(h)}) = \frac{1}{N} \sum_{i=1}^N L\left(\mathbf{y}_i, \rho\left(\bar{f}(|\mathbf{h}^{(i)}|, \mathbf{h}^{(i)}; \boldsymbol{\theta}^{(f)}); \boldsymbol{\theta}^{(\rho)}\right)\right), \quad (7)$$

where

$$\bar{f}(|\mathbf{h}^{(i)}|, \mathbf{h}^{(i)}; \boldsymbol{\theta}^{(f)}) = \frac{1}{|\mathbf{h}^{(i)}|!} \sum_{\pi \in \Pi_{|\mathbf{h}^{(i)}|}} \bar{f}(|\mathbf{h}^{(i)}|, \mathbf{h}_{\pi}^{(i)}; \boldsymbol{\theta}^{(f)}) \quad (8)$$

and  $\mathbf{h}^{(i)} = h(\mathbf{x}_i; \boldsymbol{\theta}^{(h)}) \in \mathbb{H}^{\cup}$ . Computing the gradient of equation 7 is intractable for large inputs  $\mathbf{h}^{(i)}$ , as the backpropagation computation graph branches out for every permutation in the sum. To address this computational challenge, we will turn our attention to stochastic optimization.

**Permutation sampling.** Consider replacing the Janossy sum in equation 8 with the estimate

$$\hat{\bar{f}}(|\mathbf{h}|, \mathbf{h}; \boldsymbol{\theta}^{(f)}) = \bar{f}(|\mathbf{h}|, \mathbf{h}_{\mathbf{s}}; \boldsymbol{\theta}^{(f)}), \quad (9)$$

where  $\mathbf{s}$  is a random permutation sampled uniformly,  $\mathbf{s} \sim \text{Unif}(\Pi_{|\mathbf{h}|})$ . The estimator in equation 9 is unbiased:  $E_{\mathbf{s}}[\hat{\bar{f}}(|\mathbf{h}|, \mathbf{h}_{\mathbf{s}}; \boldsymbol{\theta}^{(f)})] = \bar{f}(|\mathbf{h}|, \mathbf{h}; \boldsymbol{\theta}^{(f)})$ . Note however that when  $\bar{f}$  is chained with another nonlinear function  $\rho$  and/or nonlinear loss  $L$ , the composition is no longer unbiased:  $E_{\mathbf{s}}[L(\mathbf{y}, \rho(\hat{\bar{f}}(|\mathbf{h}_{\mathbf{s}}|, \mathbf{h}_{\mathbf{s}}; \boldsymbol{\theta}^{(f)}); \boldsymbol{\theta}^{(\rho)}))] \neq L(\mathbf{y}, \rho(E_{\mathbf{s}}[\bar{f}(|\mathbf{h}_{\mathbf{s}}|, \mathbf{h}_{\mathbf{s}}; \boldsymbol{\theta}^{(f)})]; \boldsymbol{\theta}^{(\rho)}))$ . Nevertheless, we use this estimate to propose the following stochastic approximation algorithm for gradient descent:

*Definition 2.3:* [ $\pi$ -SGD] Let  $\mathcal{B} = \{(\mathbf{x}_1, \mathbf{y}_1), \dots, (\mathbf{x}_B, \mathbf{y}_B)\}$  be a mini-batch i.i.d. sampled uniformly from the training data  $\mathcal{D}$ . At step  $t$ , consider the stochastic gradient descent update

$$\boldsymbol{\theta}_t = \boldsymbol{\theta}_{t-1} - \eta_t \mathbf{Z}_t, \quad (10)$$

where  $\mathbf{Z}_t$  is the random gradient:

$$\mathbf{Z}_t = \frac{1}{B} \sum_{(\mathbf{x}, \mathbf{y}) \in \mathcal{B}} \nabla_{\boldsymbol{\theta}} L\left(\mathbf{y}, \rho\left(\bar{f}(|\mathbf{h}^{(\mathbf{x})}|, \mathbf{h}_{\mathbf{s}_i}^{(\mathbf{x})}; \boldsymbol{\theta}_t^{(f)}); \boldsymbol{\theta}_t^{(\rho)}\right)\right),$$

and where  $\mathbf{h}^{(\mathbf{x})} \equiv h(\mathbf{x}; \boldsymbol{\theta}_t^{(h)})$ ,  $\boldsymbol{\theta} = (\boldsymbol{\theta}^{(\rho)}, \boldsymbol{\theta}^{(f)}, \boldsymbol{\theta}^{(h)})$ , with the random permutations  $\{\mathbf{s}_i\}_{i=1}^B$ , sampled independently  $\mathbf{s}_i \sim \text{Uniform}(\Pi_{|\mathbf{h}^{(i)}|})$ ; the learning rate is  $\eta_t \in (0, 1)$  s.t.  $\lim_{t \rightarrow \infty} \eta_t = 0$ ,  $\sum_{t=1}^{\infty} \eta_t = \infty$ , and  $\sum_{t=1}^{\infty} \eta_t^2 < \infty$ .  $\diamond$

Effectively, this is a Robbins-Monro stochastic approximation algorithm of gradient descent (Robbins & Monro, 1951; Bottou & LeCun, 2004) and optimizes the following modified objective func-

tion:

$$\begin{aligned} \bar{J}(\mathcal{D}; \boldsymbol{\theta}^{(\rho)}, \boldsymbol{\theta}^{(f)}, \boldsymbol{\theta}^{(h)}) &= \frac{1}{N} \sum_{i=1}^N E_{\mathbf{s}_i} \left[ L \left( \mathbf{y}_i, \rho \left( \bar{f}(|\mathbf{h}^{(i)}|, \mathbf{h}_{\mathbf{s}_i}^{(i)}; \boldsymbol{\theta}^{(f)}); \boldsymbol{\theta}^{(\rho)} \right) \right) \right] \\ &= \frac{1}{N} \sum_{i=1}^N \frac{1}{|\mathbf{h}^{(i)}|} \sum_{\pi \in \Pi_{|\mathbf{h}^{(i)}|}} L \left( \mathbf{y}_i, \rho \left( \bar{f}(|\mathbf{h}^{(i)}|, \mathbf{h}_{\pi}^{(i)}; \boldsymbol{\theta}^{(f)}); \boldsymbol{\theta}^{(\rho)} \right) \right), \end{aligned} \quad (11)$$

where  $\mathbf{h}_{\pi}^{(i)} \equiv (h(\mathbf{x}_i; \boldsymbol{\theta}^{(h)}))_{\pi}$  for a permutation  $\pi$ . Observe that the expectation over permutations is now outside the  $L$  and  $\rho$  functions. Like equation 7, the loss in equation 11 is also permutation-invariant, though we note that  $\pi$ -SGD, after a finite number of iterations, returns a  $\rho(\bar{f}(\dots, \mathbf{h}^{(i)}, \dots))$  sensitive to the random input permutations of  $\mathbf{h}^{(i)}$  presented to the algorithm. Further, unless the function  $\bar{f}$  itself is permutation-invariant ( $\bar{f} = \bar{f}$ ), the optima of  $\bar{J}$  are different from those of the original objective function  $\bar{L}$ . Instead,  $\bar{J}$  is an upper bound to  $\bar{L}$  via Jensen's inequality if  $L$  is convex and  $\rho$  is the identity function (equation 3); minimizing this upper bound forms a tractable surrogate to the original Janossy objective. If the function-class used to model  $\bar{f}$  is rich enough to include permutation-invariant functions, then the global minima of  $\bar{J}$  will include those of  $\bar{L}$ . In general, minimizing the upper bound implicitly regularizes  $\bar{f}$  to return functions that are as insensitive to the permutations of the training data. While a general  $\rho$  no longer upper bounds the original objective, the implicit regularization of permutation-sensitive functions still applies to the composition  $\bar{f}' \equiv \rho \circ \bar{f}$  and our results exhibit competitive results.

It is important to observe that the function  $\rho$  plays a very different role in our  $\pi$ -SGD formulation compared to  $k$ -ary Janossy pooling. Previously  $\rho$  was composed with an average over  $\bar{f}$  to model dependencies not captured in the average— and was in some sense separate from  $\bar{f}$  — whereas here it becomes absorbed directly into  $\bar{f}' = \rho \circ \bar{f}$ .

The next result provides some insight into the convergence properties of our algorithm.

**Proposition 2.1.** [ $\pi$ -SGD Convergence] Consider the  $\pi$ -SGD algorithm in Definition 2.3. If

- (a) there exists a constant  $M > 0$  such that for all  $\boldsymbol{\theta}$ ,  $-\mathbf{G}_t^T \boldsymbol{\theta} \leq M \|\boldsymbol{\theta} - \boldsymbol{\theta}^*\|_2^2$ , where  $\mathbf{G}_t$  is the true gradient for the full batch over all permutations,  $\mathbf{G}_t = \nabla_{\boldsymbol{\theta}} \bar{J}(\mathcal{D}; \boldsymbol{\theta}_t^{(\rho)}, \boldsymbol{\theta}_t^{(f)}, \boldsymbol{\theta}_t^{(h)})$ , where  $\boldsymbol{\theta} \equiv (\boldsymbol{\theta}^{(\rho)}, \boldsymbol{\theta}^{(f)}, \boldsymbol{\theta}^{(h)})$ , and  $\boldsymbol{\theta}^*$  is the optimum.
- (b) there exists a constant  $\delta > 0$  such that for all  $\boldsymbol{\theta}$ ,  $E_t[\|\mathbf{Z}_t\|_2^2] \leq \delta^2(1 + \|\boldsymbol{\theta}_t - \boldsymbol{\theta}_t^*\|_2^2)$ , where the expectation is taken with respect to all the data prior to step  $t$ .

Then, the algorithm in equation 10 converges to  $\boldsymbol{\theta}^*$  with probability one.

*Proof.* First, we can show that  $E_t[\mathbf{Z}_t] = \mathbf{G}_t$  by equation 11, the linearity of the derivative operator, and the fact that the permutations are independently sampled for each training example in the mini-batch and are assumed independent of  $\boldsymbol{\theta}$ . That equation 10 converges to  $\boldsymbol{\theta}^*$  is a consequence of our conditions and the supermartingale convergence theorem (Grimmett & Stirzaker, 2001, pp. 481). The following argument follows Yuille (2004). Let  $A_t = \|\boldsymbol{\theta}_t - \boldsymbol{\theta}^*\|_2^2$ ,  $B_t = \delta^2 \eta_t^2$ , and  $C_t = -\|\boldsymbol{\theta}_t - \boldsymbol{\theta}^*\|_2^2 (\delta^2 \eta_t^2 - 2M \eta_t)$ . Note that  $C_t$  is positive for a sufficiently large  $t$ , and  $\sum_{t=1}^{\infty} B_t \leq \infty$  by our definition of  $\eta_t$ . We demonstrate that  $E_t[A_t] \leq A_{t-1} + B_{t-1} - C_{t-1}$ , for all  $t$ , in the Supplementary Material. It follows that  $A_t$  converges to zero with probability one and  $\sum_{t=1}^{\infty} C_t < \infty$ .  $\square$

There are also ways to cope with the difference in objective functions between equation 7 and equation 11. An interesting approach adds an output regularization penalty for two distinct sampled permutations  $\mathbf{s}_i$  and  $\mathbf{s}'_i$ ,  $\|\bar{f}(|\mathbf{h}_{\mathbf{s}_i}|, \mathbf{h}_{\mathbf{s}_i}(\mathbf{x}^{(i)}; \boldsymbol{\theta}^{(h)}); \boldsymbol{\theta}^{(f)}); \boldsymbol{\theta}^{(\rho)} - \bar{f}(|\mathbf{h}_{\mathbf{s}'_i}|, \mathbf{h}_{\mathbf{s}'_i}(\mathbf{x}^{(i)}; \boldsymbol{\theta}^{(h)}); \boldsymbol{\theta}^{(f)}); \boldsymbol{\theta}^{(\rho)}\|_2^2$ , so as to reduce the variance of the sampled Janossy pooling output. Such a variance-reduction procedure allows  $E_{\mathbf{s}}[L(y_i, \bar{f}(|\mathbf{h}_{\mathbf{s}}|, \mathbf{h}_{\mathbf{s}}; \boldsymbol{\theta}^{(f)}))] \approx L(y_i, E_{\mathbf{s}}[\bar{f}(|\mathbf{h}_{\mathbf{s}}|, \mathbf{h}_{\mathbf{s}}; \boldsymbol{\theta}^{(f)})])$ , inducing a near-equivalence between optimizing equation 7 and equation 11, assuming  $\rho$  is the identity or  $\rho$  is combined with  $\bar{f}$  to form a single function  $\bar{f}' \equiv \rho \circ \bar{f}$ . This type of output-regularization-for-variance-reduction approach has been successfully used before to improve test performance of the average Dropout masks on LSTMs (Zolna et al., 2018).

**Inference.** The use of  $\pi$ -SGD to optimize the Janossy pooling layer optimizes the objective  $\overline{\overline{J}}$ , and thus has the following implication on how outputs should be calculated at inference time:

**Remark 2.2** (Inference). Assume  $L$  is convex (e.g.,  $L$  is the  $L^2$ , cross-entropy, or negative log-likelihood losses), which via Jensen’s inequality makes  $\pi$ -SGD a proper surrogate to the original Janossy objective. At test time we estimate the output  $\mathbf{y}_i$  of input  $\mathbf{x}_i$  by computing (or estimating)

$$\hat{\mathbf{y}}_i(\mathbf{x}_i) = E_{\mathbf{s}_i} \left[ \bar{f}^{\uparrow}(|\mathbf{h}^{(i)*}|, \mathbf{h}_{\mathbf{s}_i}^{(i)*}; \boldsymbol{\theta}^{(f')*}) \right] = \frac{1}{|\mathbf{h}^{(i)*}|} \sum_{\pi \in \Pi_{|\mathbf{h}^{(i)*}|}} \bar{f}^{\uparrow}(|\mathbf{h}^{(i)*}|, \mathbf{h}_{\pi}^{(i)*}; \boldsymbol{\theta}^{(f')*}), \quad (12)$$

where  $\bar{f}^{\uparrow} \equiv \rho \circ \bar{f}$ ,  $\boldsymbol{\theta}^{(f')*} \equiv (\boldsymbol{\theta}^{(f)*}, \boldsymbol{\theta}^{(\rho)*})$ ,  $\mathbf{h}_{\mathbf{s}_i}^{(i)*} \equiv (h(\mathbf{x}_i; \boldsymbol{\theta}^{(h)*}))_{\mathbf{s}_i}$  and  $\boldsymbol{\theta}^{(\rho)*}, \boldsymbol{\theta}^{(f)*}, \boldsymbol{\theta}^{(h)*}$  are fixed points of the  $\pi$ -SGD optimization. Equation 12 is a permutation-invariant function.

**Combining  $\pi$ -SGD and Janossy with  $k$ -ary Dependencies** In some cases one may consider  $k$ -ary Janossy pooling with a moderately large value of  $k$  in which case even the summation over  $\frac{|\mathbf{h}|!}{(|\mathbf{h}|-k)!}$  terms (see proposition 2.1) becomes expensive. In these cases, one may sample  $\mathbf{s} \sim \text{Unif}(\Pi_{|\mathbf{h}|})$  and compute  $\hat{\bar{f}}_k = \bar{f}(k, \downarrow_k(\mathbf{h}_{\mathbf{s}}); \boldsymbol{\theta}^{(f)})$  in lieu of the sum in equation 5. Note that equation 5 defining  $k$ -ary Janossy pooling constitutes exact inference of a simplified model whereas  $\pi$ -SGD with  $k$ -ary dependencies constitutes approximate inference. We will return to this idea in our results section where we note that the GraphSAGE model of Hamilton et al. (2017) can be cast as a  $\pi$ -SGD approximation of  $k$ -ary Janossy pooling.

## 2.4 PROBABILISTIC INTERPRETATION

Our work has a strong connection with finite exchangeability. Readers may be more familiar with the concept of *infinite exchangeability* through de Finetti’s theorem (De Finetti, 1937; Diaconis, 1977), which imposes strong structural requirements: the probability of any subsequence must equal the marginalized probability of the original sequence. This implies a simpler structure: sample a random variable conditioned on which all observations are independent and identically distributed. Finite exchangeability drops this projectivity requirement (Diaconis, 1977), and in general, the distribution cannot be simplified beyond first sampling the number of observations  $m$ , and then sampling their values from some general exchangeable but non-i.i.d. distribution  $p_{\text{xchg}}^m(x_1, \dots, x_m)$  (Daley & Vere-Jones, 2003).

Finite exchangeability also arises from the theory of spatial point processes; our framework of Janossy pooling is inspired by *Janossy densities* (Daley & Vere-Jones, 2003), which model the finite exchangeable distributions as mixtures of non-exchangeable distributions applied to permutations. This literature also studies simplified exchangeable point processes such as finite Gibbs models (Vo et al., 2018; Moller & Waagepetersen, 2003) that restrict the structure of  $p_{\text{xchg}}$  to fixed-order dependencies, and are related to  $k$ -ary Janossy.

## 3 EXPERIMENTS

In what follows we empirically evaluate two tractable Janossy pooling approaches,  $k$ -ary dependencies (section 2.2) and sampling permutations for stochastic optimization (section 2.3), to learn permutation-invariant functions for tasks of different complexities.

One baseline we compare against is deep sets (Zaheer et al., 2017); recall that this corresponds to unary ( $k = 1$ ) Janossy pooling (Remark 2.1). Corollary 2.1 shows that explicitly modeling higher-order dependencies during pooling simplifies the task of the upper layers ( $\rho$ ) of the neural network, and we evaluate this experimentally by letting  $k = 1, 2, 3, |\mathbf{h}|$  over different arithmetic tasks. We also evaluate Janossy pooling in graph tasks, where it can be used as a permutation-invariant function to aggregate the features and embeddings of the neighbors of a vertex in the graph. Note that in graph tasks, permutation-invariance is required to ensure that the neural network is invariant to permutations in the adjacency matrix (graph isomorphism). The code used to generate the results in this section are available on GitHub<sup>1</sup>.

<sup>1</sup><https://github.com/balasrini33/JanossyPooling>



### 3.1 ARITHMETIC TASKS ON SEQUENCES OF INTEGERS

We first consider the task of predicting the *sum* of a sequence of integers (Zaheer et al., 2017) and extend it to predicting other permutation-invariant functions: *range*, *unique sum*, *unique count*, and *variance*. In the *sum* task we predict the sum of a sequence of 5 integers drawn uniformly at random with replacement from  $\{0, 1, \dots, 99\}$ ; the *range* task also receives a sequence 5 integers distributed the same way and tries to predict the range (the difference between the maximum and minimum values); the *unique sum* task receives a sequence of 10 integers, sampled uniformly with replacement from  $\{0, 1, \dots, 9\}$ , and predicts the sum of all unique elements; the *unique count* task also receives a sequence of repeating elements, from  $\{0, 1, \dots, 9\}$ , distributed in the same way as with the *unique sum* task, and predicts the number of unique elements; the *variance* task receives a sequence of 10 integers drawn uniformly with replacement from  $\{0, 1, \dots, 99\}$  and tries to predict the variance  $\frac{1}{|\mathbf{x}|} \sum_i (x_i - \bar{x})^2 = \frac{1}{2|\mathbf{x}|^2} \sum_{i,j} (x_i - x_j)^2$ , where  $\bar{x}$  denotes the mean, of the sequence. Unlike Zaheer et al. (2017), we choose to work with the digits themselves, rather than with MNIST images. This allows a more direct assessment of the different Janossy pooling approximations, and it is a simple matter to pass digit images through another neural network layer to get an embedding  $\mathbf{h}$  before applying our algorithms. Note that computing the sum is naturally a unary task that lends itself to the approach of embedding individual digits then adding them together. However, the other tasks we selected involved calculating permutation-invariant quantities that require reasoning about high-order relationships within the sequence. Following Zaheer et al. (2017), we report accuracy (0-1 loss) for all tasks with an integer target; we report root MSE for the variance task.

We explore several Janossy pooling models. First, *Deep Sets*, or *Janossy* ( $k = 1$ ) and *Janossy*  $k = 2, 3$  where  $\vec{f}$  is a feedforward network with a single hidden layer comprised of 30 neurons. As explained in the Supplementary Material, the models are constructed to have the same number of parameters regardless of  $k$  by modifying the embedding (output) dimension of  $h$ . Second, full ( $k = |\mathbf{h}|$ ) Janossy pooling where  $\vec{f}$  is an LSTM or a GRU (50 and 80 units in the hidden state, respectively) that returns the short-term hidden state of the last temporal unit (the  $\mathbf{h}_t$  of Cho et al. with  $t = |\mathbf{h}|$ ). Recalling equation 4, we often compose the output of Janossy pooling with a function  $\rho$ . We choose two different forms for  $\rho$ : a single dense layer with identity activation (which we will call *Linear*  $\rho$ ) as with Zaheer et al. (2017) and a feedforward network with one hidden layer using tanh activations and 100 units. Choosing these forms for  $\rho$  – a simple and complex form – allows insight into the extent to which  $\rho$  supplements the capacity of the model by capturing  $\overline{\overline{\mathbf{J}}}$  relationships not exploited during pooling, and serves as an evaluation of the strategy of optimizing  $\overline{\overline{\mathbf{J}}}$  as a tractable approximation of  $\overline{\overline{\mathbf{L}}}$ . Inference for the  $k$ -ary models is exact, but when  $k = |\mathbf{h}|$  and  $\vec{f}$  is an RNN, we use approximate  $\pi$ -SGD inference; we experiment with estimating equation 12 using 1 and 20 sampled permutations at inference time.

Much of our implementation, architectural, and experimental design are based on the deep sets code<sup>2</sup> of Zaheer et al. (2017): please see the Supplementary Material for further details. We tuned the Adam learning rate for each model and report the results using the rate yielding top performance on the validation set. Table 1 shows the accuracy (average 0-1 loss) of all tasks except variance, for which we report Root-MSE in Table 2. We trained each model with 15 random initializations of the weights to quantify variability. Table 4 in the Supplementary Material shows the same results measured by mean absolute error. The data consists of 100,000 training examples and 10,000 test examples.

We see that models trained with  $\pi$ -SGD using an RNN as  $\vec{f}$  typically achieve top performance or are comparable to the top performer on all tasks, for either choice of  $\rho$ . We also observe for these models that adding complexity to  $\rho$  can yield small but meaningful performance gains or maintain similar performance, lending credence to the approach of optimizing  $\overline{\overline{\mathbf{J}}}$  as a tractable approximation to  $\overline{\overline{\mathbf{L}}}$ . Since performance is rather saturated for these tasks, it is difficult to evaluate the impact of increasing the number of test-time permutation samples, but we see that it improves performance in the range task with LSTM and a linear  $\rho$  – please see Section 3.2 for more related results. We can also observe that deep sets pushes complexity to  $\rho$  when tasks require reasoning within elements in the set from the difference in performance between a linear and MLP  $\rho$ . Last, we observe counterintuitive results for Janossy  $k = 2, 3$ ; adding a hidden layer to  $\rho$  deteriorates performance on the sum task. This is likely an issue with the optimization as adding an additional layer to  $\rho$  should in theory never

<sup>2</sup><https://github.com/manzilzaheer/DeepSets>

Table 1: Accuracy (average 0-1 loss) of various Janossy pooling approximations under distinct tasks. The *method* column refers to the inference strategy utilized. *Inf sample* refers to the number of permutations sampled at test time to estimate equation 12 for methods learned with  $\pi$ -SGD.  $k = 1$  corresponds to Deepsets. tanh activations are used with the MLP. Standard deviations computed over 15 runs are shown in parentheses.

$\vec{f}$	<i>method</i>	<i>inf sample</i>	$k$	$\rho$	<i>sum</i>	<i>range</i>	<i>unique sum</i>	<i>unique count</i>
MLP (30)	exact	N.A.	1	Linear	1.000(0.000)	0.039(0.001)	0.075(0.002)	0.358(0.005)
MLP (30)	exact	N.A.	2	Linear	0.999(0.001)	0.088(0.003)	0.173(0.004)	0.736(0.029)
MLP (30)	exact	N.A.	3	Linear	0.990(0.003)	0.206(0.004)	0.438(0.021)	0.889(0.040)
MLP (30)	exact	N.A.	1	MLP (100)	0.990(0.010)	0.964(0.008)	1.000(0.000)	1.000(0.000)
MLP (30)	exact	N.A.	2	MLP (100)	0.506(0.146)	0.861(0.021)	1.000(0.000)	1.000(0.000)
MLP (30)	exact	N.A.	3	MLP (100)	0.242(0.035)	0.809(0.034)	1.000(0.000)	1.000(0.000)
LSTM(50)	$\pi$ -SGD	1	n	Linear	0.997(0.002)	0.955(0.009)	1.000(0.000)	1.000(0.000)
LSTM(50)	$\pi$ -SGD	20	n	Linear	0.999(0.000)	0.970(0.006)	1.000(0.000)	1.000(0.000)
GRU(80)	$\pi$ -SGD	1	n	Linear	0.993(0.012)	0.983(0.004)	1.000(0.000)	1.000(0.000)
GRU(80)	$\pi$ -SGD	20	n	Linear	0.999(0.002)	0.989(0.002)	1.000(0.000)	1.000(0.000)
LSTM(50)	$\pi$ -SGD	1	n	MLP (100)	0.993(0.010)	0.995(0.001)	1.000(0.000)	1.000(0.000)
LSTM(50)	$\pi$ -SGD	20	n	MLP (100)	0.996(0.006)	0.996(0.001)	1.000(0.000)	1.000(0.000)
GRU(80)	$\pi$ -SGD	1	n	MLP (100)	0.998(0.004)	0.998(0.001)	1.000(0.000)	1.000(0.000)
GRU(80)	$\pi$ -SGD	20	n	MLP (100)	0.998(0.004)	0.998(0.001)	1.000(0.000)	1.000(0.000)

Table 2: Root-MSE of various Janossy pooling approximations for the variance task. The columns other than *variance* are identical to those in Table 1.

$\vec{f}$	<i>method</i>	<i>inf sample</i>	$k$	$\rho$	<i>variance</i>
MLP (30)	exact	N.A.	1	Linear	119.051(1.295)
MLP (30)	exact	N.A.	2	Linear	4.369(0.501)
MLP (30)	exact	N.A.	3	Linear	8.993(0.995)
MLP (30)	exact	N.A.	1	MLP (100)	2.405(0.588)
MLP (30)	exact	N.A.	2	MLP (100)	11.582(4.121)
MLP (30)	exact	N.A.	3	MLP (100)	47.986(3.094)
LSTM(50)	$\pi$ -SGD	1	n	Linear	1.649(0.222)
LSTM(50)	$\pi$ -SGD	20	n	Linear	1.394(0.256)
GRU(80)	$\pi$ -SGD	1	n	Linear	1.427(0.23)
GRU(80)	$\pi$ -SGD	20	n	Linear	1.199(0.23)
LSTM(50)	$\pi$ -SGD	1	n	MLP (100)	1.054(0.77)
LSTM(50)	$\pi$ -SGD	20	n	MLP (100)	1.022(0.41)
GRU(80)	$\pi$ -SGD	1	n	MLP (100)	0.421(0.62)
GRU(80)	$\pi$ -SGD	20	n	MLP (100)	0.398(0.37)

degrade performance. Janossy  $k = 2, 3$  also performs worse than  $k = 1$  with when  $\rho$  is an MLP on the range task, likely another learning issue since we know theoretically that  $k$ -ary Janossy pooling is more expressive than  $(k - 1)$ -ary.

### 3.2 JANOSSY POOLING AS AN AGGREGATOR FUNCTION FOR VERTEX CLASSIFICATION

Here we consider Janossy pooling in the context of graph neural networks to learn vertex representations enabling vertex classification. The GraphSAGE (SAmple and aggreGatE) algorithm (Hamilton et al., 2017) consists of sampling vertex attributes from the neighbor set of each vertex  $v$  before performing an aggregation operation which generates an embedding of  $v$ ; the authors consider permutation-invariant operations such as mean and max as well as the permutation-sensitive operation of feeding a randomly permuted neighborhood sequence to an LSTM. The sample and aggregate procedure is repeated twice to generate an embedding. Each step can be considered as Janossy pooling with  $\pi$ -SGD with  $k$ -ary subsequences, where  $k_l, l \in \{1, 2\}$  is the number of vertices sampled from each neighborhood and  $\vec{f}$  is for instance a mean, max, or LSTM. However, at test time, GraphSAGE only samples one permutation  $s$  of each neighborhood to estimate equation 12.

Table 3: Performance (Micro-F1) using Janossy pooling with  $k$ -ary subsets and  $\pi$ -SGD in a graph neural network – GraphSAGE– with 20 permutations sampled at test time. Standard deviations over 30 runs for Cora/Pubmed and 4 runs for PPI are shown in parentheses.

$\bar{f}$	method	$k_1$	$k_2$	CORA	PUBMED	PPI
LSTM	$\pi$ -SGD	3	3	0.860 (.009)	0.889 (0.009)	0.538 (.005)
LSTM	$\pi$ -SGD	5	5	– <sup>a</sup>	– <sup>a</sup>	0.579 (.015)
LSTM	$\pi$ -SGD	10	25	– <sup>a</sup>	– <sup>a</sup>	0.650 (.013)
LSTM	$\pi$ -SGD	25	10	– <sup>a</sup>	– <sup>a</sup>	0.689 (.062)
LSTM	$\pi$ -SGD	25	25	– <sup>a</sup>	– <sup>a</sup>	0.702 (.044)
LSTM	$\pi$ -SGD	Full	Full	– <sup>a</sup>	– <sup>a</sup>	0.757 (.040) <sup>b</sup>
Mean-Pooling	exact	Full	Full	0.860 (.008)	0.881 (.011)	0.767 (.013)

<sup>a</sup> Entries denoted by – all differ by less than 0.01. The typical neighborhoods in Cora and Pubmed are small, so that sampling  $\geq 5$  neighbors is often equivalent to using the entire neighborhood.

<sup>b</sup> Some neighbor sequences in PPI are prohibitively large, so we take  $k_1 = k_2 = 100$ .

In this section we investigate the impact of increasing  $k$  and the number of sampled permutations  $s$  on performance. To implement the model and design our experiments, we modified the reference PyTorch code<sup>3</sup> provided by the authors and referred to the TensorFlow code associated with the original publication<sup>4</sup>. Wherever we found discrepancies between the code and original publication, we followed the code; please see the Supplementary Material for further implementation details. We consider three datasets: Cora and Pubmed (Sen et al., 2008) – smaller graphs included in the aforementioned PyTorch repository – and the larger Protein-Protein Interaction (PPI) (Zitnik & Leskovec, 2017) graphs considered in Hamilton et al. (2017). The first two are citation networks where vertices represent papers, edges represent citations, and vertex features are bag-of-words representations of the document text. The task is to classify the paper topic. The PPI dataset is a collection of several graphs each representing human tissue; vertices represent proteins, edges represent protein interaction, features include genetic and immunological features, and we try to classify protein roles. More details of these datasets and our experimental test/train splits are shown in Table 6 in the Supplementary Material.

Given that the average degree of Cora and Pubmed are less than 5 and that of PPI is 28.8, and that the original GraphSAGE paper sampled 10 and 25 neighbors, we consider models where  $k_1, k_2 \in \{3, 5, 10, 25\}$ . We model  $\bar{f}$  as an LSTM and a mean. Note that the number of parameters in the model is independent of  $k$  when we take  $\bar{f}$  to be an LSTM. At inference time, we sample 20 random permutations of each sequence and average the predicted probabilities before making a final class vote. Our models and results are shown in Table 3. Note that the choice of  $k \in \{5, 10, 25\}$  makes little difference on Cora and Pubmed due to the small neighborhood sizes:  $k \geq 5$  often amounts to sampling the entire neighborhood. With PPI, increasing  $k$  yields consistent improvement. The strong performance of Mean Pooling points to both a relatively easy task and the benefits of utilizing the entire neighborhood of each vertex. It is reasonable to suppose that the topic of a paper can be adequately predicted by computing the average bag-of-words representations of papers in the neighborhood without reasoning about relationships between neighboring papers; suppose for instance that every paper in the neighborhood contains frequent mention of the word *neural*. Figure 2 shows the mean performance – across models trained with four random initializations – for each model using varying numbers of sampled permutations  $s \sim \Pi_{|h|}$  at test time. Increasing the number of sampled permutations yields consistent improvement. The benefits start to level off but sampling more permutations does not risk degrading performance. The effect is stronger when  $k$  is larger. Paired tests – t and Wilcoxon signed rank – of the hypothesis that the mean difference in performance between 7 sampled permutations – where the gains level off – versus 1 using  $k_1 = k_2 = 25$  and 12 replicates are significant with  $p < 10^{-3}$ . The test was performed with  $k_1 = k_2 = 25$  due to the computational burden of training with  $k_1 = k_2 = 100$ .

## 4 RELATED WORK

Under the Janossy pooling framework presented in this work, existing literature falls under one of three approaches to approximating to the intractable Janossy-pooling layer: *Canonical orderings*, *k-ary dependencies*, and *permutation sampling*.

<sup>3</sup><https://github.com/williamleif/graphsage-simple/>

<sup>4</sup><https://github.com/williamleif/GraphSAGE>

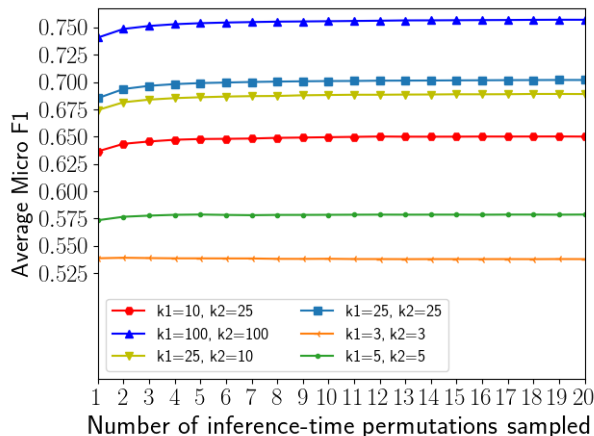


Figure 2: Mean performance vs number of permutations sampled at test time, PPI task,  $\overrightarrow{f} = \text{LSTM}$

**Canonical Ordering Approaches.** In section 2.1, we saw how permutation invariance can be achieved by mapping permutations to a canonical ordering. Rather than trying to define a good canonical ordering, one can try to learn it from the data, however searching among all  $|\mathbf{h}|!$  permutations for one that correlates with the task of interest is a difficult discrete optimization problem. Recently, Rezatofighi et al. (2018) proposed a method that computes the posterior distribution of all permutations, conditioned on the model and the data. This posterior-sampling approach is intractable for large inputs, unfortunately. We note in passing that Rezatofighi et al. (2018) is interested in permutation-invariant outputs, and that Janossy pooling is also trivially applicable to these tasks. Vinyals et al. (2016) proposes a heuristic using ancestral sampling while learning the model.

**$k$ -ary Janossy Pooling Approaches.** In section 2.2 we described  $k$ -ary Janossy pooling, which considers  $k$ -order relationships in the input vector  $\mathbf{h}$  to simplify optimization. Deep Sets (Zaheer et al., 2017) can be characterized as unary Janossy pooling (i.e.,  $k$ -ary for  $k = 1$ ). Ravanbakhsh et al. (2017) proposes a similar unary Janossy pooling to *deep sets*. Cotter et al. (2018) proposes to add inductive biases to the *deep sets* model in the form of monotonicity constraints with respect to the vector valued elements of the input sequence by modeling  $\phi$  and  $\rho$  with Deep Lattice Networks (You et al., 2017); one can extend Cotter et al. (2018) by using higher-order  $k$ -ary Janossy pooling with  $k > 1$ .

Exploiting dependencies within a sequence to learn a permutation-invariant function has been discussed elsewhere. For instance Santoro et al. (2017) exploits pairwise relationships to perform relational reasoning about pairs of objects in an image and Battaglia et al. (2018) contemplates modeling the center of mass of a solar system by including the pairwise interactions among planets. However, Janossy pooling provides a general framework for capturing dependencies within a permutation-invariant pooling layer.

**Permutation Sampling Approaches.** In section 2.3 we have seen that permutation sampling can be used as a stochastic gradient procedure ( $\pi$ -SGD) to learn a model with a Janossy pooling layer. The learned model provides only an approximate solution to original permutation-invariant function. Permutation sampling has been used as a heuristic (without a theoretical justification) in both Moore & Neville (2017) and Hamilton et al. (2017), which found that randomly permuting sequences and feeding them forward to an LSTM is effective in relational learning tasks that require permutation-invariant pooling layers.

## 5 CONCLUSIONS

Our approach of permutation-invariance through Janossy pooling unifies a number of existing approaches, and opens up avenues to develop both new methodological extensions, as well as better theory. Our paper focused on two main approaches:  $k$ -ary interactions and random permutations. The former involves exact Janossy pooling for a restricted class of functions  $\overrightarrow{f}$ . Adding an additional

neural network  $\rho$  can recover lost model capacity, but now hurts tractability and identifiability. Placing restrictions on  $\rho$  (convexity, Lipschitz continuity etc.) can allow a more refined control of this trade-off, allowing theoretical and empirical work to shed light on the compromises involved. The second was a random permutation approach which conversely involves no clear trade-offs between model capacity and computation when  $\rho$  is made more complex, instead it modifies the relationship between the tractable approximate loss  $\bar{J}$  and the original Janossy loss  $\bar{L}$ . While the difference between  $\bar{J}$  and  $\bar{L}$  reduces as more permutations are sampled and we saw strong empirical performance of this approach in our experiments, identifying which problems it is best suited for is an opportunity for future work. Further, a better understanding how the loss-functions  $\bar{L}$  and  $\bar{J}$  relate to each other can shed light on the slightly black-box nature of this procedure. It is also important to understand the relationship between the random permutation approach to canonical ordering and how one might be used to improve the other. Finally, it is important to apply our methodology to a wider range of applications. Two immediate domains are more challenging tasks involving graphs and tasks involving non-Poisson point processes.

## REFERENCES

- James Atwood and Don Towsley. Diffusion-convolutional neural networks. In *NIPS*, 2016.
- Peter W Battaglia, Jessica B Hamrick, Victor Bapst, Alvaro Sanchez-Gonzalez, Vinicius Zambaldi, Mateusz Malinowski, Andrea Tacchetti, David Raposo, Adam Santoro, Ryan Faulkner, et al. Relational inductive biases, deep learning, and graph networks. *arXiv preprint arXiv:1806.01261*, 2018.
- Léon Bottou and Yann LeCun. Large scale online learning. In *NIPS*, 2004.
- Kyunghyun Cho, Bart Van Merriënboer, Caglar Gulcehre, Dzmitry Bahdanau, Fethi Bougares, Holger Schwenk, and Yoshua Bengio. Learning phrase representations using rnn encoder-decoder for statistical machine translation. *EMNLP*, 2014.
- François Chollet et al. Keras. <https://keras.io>, 2015.
- Andrew Cotter, Maya Gupta, Heinrich Jiang, James Muller, Taman Narayan, Serena Wang, and Tao Zhu. Interpretable set functions. *arXiv preprint arXiv:1806.00050*, 2018.
- Daryl J Daley and David Vere-Jones. *An introduction to the theory of point processes: volume II: general theory and structure*. Springer, 2003.
- Bruno De Finetti. La prévision: ses lois logiques, ses sources subjectives. In *Annales de l'institut Henri Poincaré*, volume 7, pp. 1–68, 1937. [Translated into English: H. E. Kyburg and H.E. Smokler, eds. *Studies in Subjective Probability. Krieger* 53-118, 1980].
- Persi Diaconis. Finite forms of de Finetti’s theorem on exchangeability. *Synthese*, 36(2):271–281, 1977.
- David K. Duvenaud, Dougal Maclaurin, Jorge Iparraguirre, Rafael Bombarell, Timothy Hirzel, Alan Aspuru-Guzik, and Ryan P. Adams. Convolutional Networks on Graphs for Learning Molecular Fingerprints. In *NIPS*, 2015.
- Justin Gilmer, Samuel S. Schoenholz, Patrick F. Riley, Oriol Vinyals, and George E. Dahl. Neural message passing for quantum chemistry. In *ICML*, 2017.
- Geoffrey Grimmett and David Stirzaker. *Probability and random processes*. Oxford university press, 2001.
- William L. Hamilton, Rex Ying, and Jure Leskovec. Inductive Representation Learning on Large Graphs. In *NIPS*, jun 2017. URL <http://arxiv.org/abs/1706.02216>.
- Sepp Hochreiter and Jürgen Schmidhuber. Long short-term memory. *Neural computation*, 9(8): 1735–1780, 1997.
- Glen Jeh and Jennifer Widom. Scaling personalized web search. In *Proceedings of the 12th international conference on World Wide Web*, pp. 271279, 2003. Citation Key: jeh2003scaling bibtex[organization=Acm].
- Diederik P. Kingma and Jimmy Lei Ba. ADAM: A Method for Stochastic Optimization. *International Conference on Learning Representations, ICLR*, 2015.
- Thomas N. Kipf and Max Welling. Semi-Supervised Classification with Graph Convolutional Networks. sep 2016. URL <http://arxiv.org/abs/1609.02907>.
- Yann LeCun, Yoshua Bengio, et al. Convolutional networks for images, speech, and time series. *The handbook of brain theory and neural networks*, 3361(10):1995, 1995.
- Yann LeCun, Yoshua Bengio, and Geoffrey Hinton. Deep learning. *Nature*, 2015.
- David Liben-Nowell and Jon Kleinberg. The link-prediction problem for social networks. *Journal of the American society for information science and technology*, 58(7):1019–1031, 2007.
- Ziqi Liu, Chaochao Chen, Longfei Li, Jun Zhou, Xiaolong Li, and Le Song. Geniepath: Graph neural networks with adaptive receptive paths. *arXiv preprint arXiv:1802.00910*, 2018.

- Jesper Moller and Rasmus Plenge Waagepetersen. *Statistical inference and simulation for spatial point processes*. Chapman and Hall/CRC, 2003.
- Federico Monti, Davide Boscaini, Jonathan Masci, Emanuele Rodola, Jan Svoboda, and Michael M Bronstein. Geometric deep learning on graphs and manifolds using mixture model cnns. In *Proc. CVPR*, volume 1, pp. 3, 2017.
- John Moore and Jennifer Neville. Deep collective inference. In *AAAI*, pp. 2364–2372, 2017.
- Mathias Niepert, Mohamed Ahmed, and Konstantin Kutzkov. Learning convolutional neural networks for graphs. In *International conference on machine learning*, pp. 2014–2023, 2016.
- Lawrence Page, Sergey Brin, Rajeev Motwani, and Terry Winograd. *The PageRank citation ranking: Bringing order to the web*. 1999.
- Siamak Ravanbakhsh, Jeff Schneider, and Barnabas Poczos. Deep Learning with Sets and Point Clouds. In *ICLR Workshop Track*, nov 2017. URL <http://arxiv.org/abs/1611.04500>.
- S Hamid Rezaatofghi, Roman Kaskman, Farbod T Motlagh, Qinfeng Shi, Daniel Cremers, Laura Leal-Taixé, and Ian Reid. Deep perm-set net: Learn to predict sets with unknown permutation and cardinality using deep neural networks. *arXiv preprint arXiv:1805.00613*, 2018.
- H. Robbins and S. Monro. A stochastic approximation method. *Annals of Mathematical Statistics*, 1951.
- Adam Santoro, David Raposo, David G Barrett, Mateusz Malinowski, Razvan Pascanu, Peter Battaglia, and Tim Lillicrap. A simple neural network module for relational reasoning. In *Advances in neural information processing systems*, pp. 4967–4976, 2017.
- Prithviraj Sen, Galileo Namata, Mustafa Bilgic, Lise Getoor, Brian Galligher, and Tina Eliassi-Rad. Collective classification in network data. *AI magazine*, 29(3):93, 2008.
- Rianne van den Berg, Thomas N Kipf, and Max Welling. Graph convolutional matrix completion. *stat*, 1050:7, 2017.
- Petar Velickovic, Guillem Cucurull, Arantxa Casanova, Adriana Romero, Pietro Lio, and Yoshua Bengio. Graph attention networks. *arXiv preprint arXiv:1710.10903*, 2017.
- Oriol Vinyals, Samy Bengio, and Manjunath Kudlur. Order Matters: Sequence to Sequence for Sets. *ICLR*, 2016.
- Ba-Ngu Vo, Nhan Dam, Dinh Phung, Quang N Tran, and Ba-Tuong Vo. Model-based learning for point pattern data. *Pattern Recognition*, 84:136–151, 2018.
- Keyulu Xu, Chengtao Li, Yonglong Tian, Tomohiro Sonobe, Ken-ichi Kawarabayashi, and Stefanie Jegelka. Representation Learning on Graphs with Jumping Knowledge Networks. In *ICML*, 2018. URL <http://arxiv.org/abs/1806.03536>.
- Rex Ying, Jiaxuan You, Christopher Morris, Xiang Ren, William L Hamilton, and Jure Leskovec. Hierarchical graph representation learning with differentiable pooling. *arXiv preprint arXiv:1806.08804*, 2018.
- Seungil You, David Ding, Kevin Canani, Jan Pfeifer, and Maya Gupta. Deep lattice networks and partial monotonic functions. In *Advances in Neural Information Processing Systems*, pp. 2981–2989, 2017.
- Alan Yuille. The Convergence of Contrastive Divergences. In *NIPS*, 2004.
- Manzil Zaheer, Satwik Kottur, Siamak Ravanbakhsh, Barnabas Poczos, Ruslan Salakhutdinov, and Alexander Smola. Deep Sets. In *NIPS*, 2017.
- Marinka Zitnik and Jure Leskovec. Predicting multicellular function through multi-layer tissue networks. *Bioinformatics*, 33(14):i190–i198, 2017.
- Konrad Zolna, Devansh Arpit, Dendi Suhbudy, and Yoshua Bengio. Fraternal dropout. *ICLR*, 2018.

## A PROOFS OF RESULTS

We restate and prove the remaining portion of Theorem 2.1.

**Theorem 2.1.** *For any  $k \in \mathbb{N}$ , define  $\mathcal{F}_k$  as the set of all permutation-invariant functions that can be represented by Janossy pooling with  $k$ -ary dependencies. Then,  $\mathcal{F}_{k-1}$  is a proper subset of  $\mathcal{F}_k$  if the space  $\mathbb{H}$  is not trivial (i.e. if the cardinality of  $\mathbb{H}$  is greater than 1). Thus, Janossy pooling with  $k$ -ary dependencies can express any Janossy pooling function with  $(k-1)$ -ary dependencies, but the converse does not hold.*

*Proof.* ( $\mathcal{F}_k \not\subset \mathcal{F}_{k-1}$ ):

As noted previously, the case where  $k = 1$  is trivial, so assume  $k > 1$ . We will demonstrate the existence of  $\bar{f}_k \in \mathcal{F}_k$  such that  $\bar{f}_{k-1} \neq \bar{f}_k$  for all  $\bar{f}_{k-1} \in \mathcal{F}_{k-1}$ . Let  $\bar{f}_k$  and  $\bar{f}_{k-1}$  be associated with  $\hat{f}_k$  and  $\hat{f}_{k-1}$ , respectively.

It suffices to consider  $|\mathbf{h}| = k$ . Let  $\hat{f}_k(|\mathbf{h}|, \mathbf{h}_\pi; \boldsymbol{\theta}_k^{(f)}) = \prod_{l=1}^{|\mathbf{h}|} h_{\pi(l)}$  whence  $\bar{f}_k(|\mathbf{h}|, \mathbf{h}; \boldsymbol{\theta}_k^{(f)}) = \prod_{l=1}^{|\mathbf{h}|} h_l$ . Thus, for any  $\bar{f}_{k-1}$  and any  $\boldsymbol{\theta}_{k-1}^{(f)}$ ,

$$\begin{aligned} \frac{\bar{f}_{k-1}(|\mathbf{h}|, \mathbf{h}; \boldsymbol{\theta}_{k-1}^{(f)})}{\bar{f}_k(|\mathbf{h}|, \mathbf{h}; \boldsymbol{\theta}_k^{(f)})} &= \frac{1}{|\mathbf{h}|!} \sum_{\pi \in \Pi_{|\mathbf{h}|}} \frac{\hat{f}_{k-1}(|\mathbf{h}|, \downarrow_{k-1}(\mathbf{h}_\pi); \boldsymbol{\theta}_{k-1}^{(f)})}{\prod_{l=1}^{|\mathbf{h}|} h_l} \\ &= \frac{1}{|\mathbf{h}|!} \sum_{j=1}^{|\mathbf{h}|} \sum_{\tilde{\pi} \in \Pi_{\{1, \dots, |\mathbf{h}|\} \setminus j}} \frac{\hat{f}_{k-1}(|\mathbf{h}|, (\mathbf{h}_{-j})_{\tilde{\pi}}; \boldsymbol{\theta}_{k-1}^{(f)})}{\prod_{l=1}^{|\mathbf{h}|} h_l} \end{aligned}$$

where  $\Pi_{\{1, \dots, |\mathbf{h}|\} \setminus j}$  is the set of permutation functions of  $\{1, 2, \dots, j-1, j+1, \dots, |\mathbf{h}|\}$  and  $(\mathbf{h}_{-j})_{\tilde{\pi}}$  is a permutation of  $\{h_1, \dots, h_{j-1}, h_{j+1}, \dots, h_{|\mathbf{h}|}\}$ . This can be written as

$$\frac{1}{|\mathbf{h}|!} \sum_{j=1}^{|\mathbf{h}|} \frac{1}{h_j} \underbrace{\left( \sum_{\tilde{\pi} \in \Pi_{\{1, \dots, |\mathbf{h}|\} \setminus j}} \frac{\hat{f}_{k-1}(|\mathbf{h}|, (\mathbf{h}_{-j})_{\tilde{\pi}}; \boldsymbol{\theta}_{k-1}^{(f)})}{\prod_{l \neq j} h_l} \right)}_{\text{denote by } a_{j, |\mathbf{h}|}},$$

therefore

$$\frac{\bar{f}_{k-1}(|\mathbf{h}|, \mathbf{h}_\pi; \boldsymbol{\theta}_{k-1}^{(f)})}{\bar{f}_k(|\mathbf{h}|, \mathbf{h}_\pi; \boldsymbol{\theta}_k^{(f)})} = \frac{1}{|\mathbf{h}|!} \sum_{j=1}^{|\mathbf{h}|} \frac{1}{h_j} a_{j, |\mathbf{h}|}. \quad (13)$$

Now,  $\bar{f}_{k-1} = \bar{f}_k$  if and only if their quotient in equation 13 is unity for all  $\mathbf{h}$ . But this is clearly not possible in general unless  $\mathbb{H}$  is a singleton, which we have precluded in our assumptions.  $\square$

Next we complete the proof of Proposition 2.1

**Proposition 2.1.** [ $\pi$ -SGD Convergence] *Consider the  $\pi$ -SGD algorithm in Definition 2.3. If*

- (a) *there exists a constant  $M > 0$  such that for all  $\boldsymbol{\theta}$ ,  $-\mathbf{G}_t^T \boldsymbol{\theta} \leq M \|\boldsymbol{\theta} - \boldsymbol{\theta}^*\|_2^2$ , where  $\mathbf{G}_t$  is the true gradient for the full batch over all permutations,  $\mathbf{G}_t = \nabla_{\boldsymbol{\theta}} \bar{J}(\mathcal{D}; \boldsymbol{\theta}_t^{(\rho)}, \boldsymbol{\theta}_t^{(f)}, \boldsymbol{\theta}_t^{(h)})$ , where  $\boldsymbol{\theta} \equiv (\boldsymbol{\theta}^{(\rho)}, \boldsymbol{\theta}^{(f)}, \boldsymbol{\theta}^{(h)})$ , and  $\boldsymbol{\theta}^*$  is the optimum.*
- (b) *there exists a constant  $\delta > 0$  such that for all  $\boldsymbol{\theta}$ ,  $E_t[\|\mathbf{Z}_t\|_2^2] \leq \delta^2(1 + \|\boldsymbol{\theta}_t - \boldsymbol{\theta}_t^*\|_2^2)$ , where the expectation is taken with respect to all the data prior to step  $t$ .*

*Then, the algorithm in equation 10 converges to  $\boldsymbol{\theta}^*$  with probability one.*

*Proof.* To complete the proof, we needed to show that if  $A_t = \|\boldsymbol{\theta}_t - \boldsymbol{\theta}^*\|_2^2$ ,  $B_t = \delta^2 \eta_t^2$ , and  $C_t = -\|\boldsymbol{\theta}_t - \boldsymbol{\theta}^*\|_2^2(\delta^2 \eta_t^2 - 2M \eta_t)$ , then  $E_t[A_t] \leq A_{t-1} + B_{t-1} - C_{t-1}$  for all  $t$ . We write

$$\begin{aligned} E_t[\|\boldsymbol{\theta}_t - \boldsymbol{\theta}^*\|_2^2] &= E_t[\|\boldsymbol{\theta}_{t-1} - \eta_{t-1} \mathbf{Z}_{t-1} - \boldsymbol{\theta}^*\|_2^2] \\ &= \|\boldsymbol{\theta}_{t-1} - \boldsymbol{\theta}^*\|_2^2 - 2\eta_{t-1} E_t[(\boldsymbol{\theta}_{t-1} - \boldsymbol{\theta}^*)^T \mathbf{Z}_{t-1}] + \eta_{t-1}^2 E_t[\|\mathbf{Z}_{t-1}\|_2^2] \\ &\leq \|\boldsymbol{\theta}_{t-1} - \boldsymbol{\theta}^*\|_2^2 - 2\eta_{t-1} (\boldsymbol{\theta}_{t-1} - \boldsymbol{\theta}^*)^T \mathbf{G}_{t-1} + \delta^2 \eta_{t-1}^2 + \delta^2 \eta_{t-1}^2 \|\boldsymbol{\theta}_{t-1} - \boldsymbol{\theta}^*\|_2^2 \\ &\leq \|\boldsymbol{\theta}_{t-1} - \boldsymbol{\theta}^*\|_2^2 - 2M \eta_{t-1} \|\boldsymbol{\theta}_{t-1} - \boldsymbol{\theta}^*\|_2^2 + \delta^2 \eta_{t-1}^2 + \delta^2 \eta_{t-1}^2 \|\boldsymbol{\theta}_{t-1} - \boldsymbol{\theta}^*\|_2^2, \end{aligned}$$

and the result follows.  $\square$



Table 4: Mean Absolute Error of various Janossy pooling approximations under distinct tasks. The column method refers to the tractability strategy. Inf sample refers to the number of permutations sampled to estimate equation 12 for methods learned with  $\pi$ -SGD.  $k = 1$  corresponds to Deepsets. tanh activations are used with the MLP’s. Standard deviations computed over 15 runs are shown in parentheses.

$\vec{f}$	method	inf sample	k	$\rho$	sum	range	unique sum	unique count
MLP (30)	exact	N.A.	1	Linear	0.0(0.0)	9.366(0.094)	4.209(0.025)	0.828(0.008)
MLP (30)	exact	N.A.	2	Linear	0.006(0.011)	4.143(0.041)	1.968(0.016)	0.277(0.029)
MLP (30)	exact	N.A.	3	Linear	0.037(0.031)	2.307(0.074)	0.73(0.04)	0.114(0.04)
MLP (30)	exact	N.A.	1	MLP (100)	0.022(0.033)	0.04(0.011)	0.0(0.0)	0.0(0.0)
MLP (30)	exact	N.A.	2	MLP (100)	0.667(0.294)	0.199(0.035)	0.0(0.0)	0.0(0.0)
MLP (30)	exact	N.A.	3	MLP (100)	1.54(0.15)	0.571(0.114)	0.0(0.0)	0.0(0.0)
LSTM(50)	$\pi$ -SGD	1	n	Linear	0.003(0.002)	0.051(0.01)	0.0(0.0)	0.0(0.0)
LSTM(50)	$\pi$ -SGD	20	n	Linear	0.001(0.001)	0.035(0.006)	0.0(0.0)	0.0(0.0)
GRU(80)	$\pi$ -SGD	1	n	Linear	0.007(0.012)	0.02(0.005)	0.0(0.0)	0.0(0.0)
GRU(80)	$\pi$ -SGD	20	n	Linear	0.001(0.002)	0.014(0.004)	0.0(0.0)	0.0(0.0)
LSTM(50)	$\pi$ -SGD	1	n	MLP (100)	0.007(0.01)	0.006(0.001)	0.0(0.0)	0.0(0.0)
LSTM(50)	$\pi$ -SGD	20	n	MLP (100)	0.004(0.006)	0.005(0.001)	0.0(0.0)	0.0(0.0)
GRU(80)	$\pi$ -SGD	1	n	MLP (100)	0.002(0.004)	0.002(0.001)	0.0(0.0)	0.0(0.0)
GRU(80)	$\pi$ -SGD	20	n	MLP (100)	0.002(0.003)	0.002(0.001)	0.0(0.0)	0.0(0.0)

Table 5: Mean Absolute Error of various Janossy pooling approximations for the variance task. The column method refers to the tractability strategy. Inf sample refers to the number of permutations sampled to estimate equation 12 for methods learned with  $\pi$ -SGD.  $k = 1$  corresponds to Deepsets. tanh activations are used with the MLP’s. Standard deviations computed over 15 runs are shown in parentheses.

$\vec{f}$	method	inf sample	k	$\rho$	variance
MLP (30)	exact	N.A.	1	Linear	69.953(0.492)
MLP (30)	exact	N.A.	2	Linear	2.262(0.363)
MLP (30)	exact	N.A.	3	Linear	6.747(0.871)
MLP (30)	exact	N.A.	1	MLP (100)	1.111(0.283)
MLP (30)	exact	N.A.	2	MLP (100)	7.779(2.902)
MLP (30)	exact	N.A.	3	MLP (100)	34.813(2.17)
LSTM(50)	$\pi$ -SGD	1	n	Linear	0.801(0.2)
LSTM(50)	$\pi$ -SGD	20	n	Linear	0.698(0.412)
GRU(80)	$\pi$ -SGD	1	n	Linear	0.795(0.205)
GRU(80)	$\pi$ -SGD	20	n	Linear	0.672(0.332)
LSTM(50)	$\pi$ -SGD	1	n	MLP (100)	0.604(0.078)
LSTM(50)	$\pi$ -SGD	20	n	MLP (100)	0.422(0.102)
GRU(80)	$\pi$ -SGD	1	n	MLP (100)	0.594(0.634)
GRU(80)	$\pi$ -SGD	20	n	MLP (100)	0.517(0.084)

## B EXPERIMENTS: FURTHER RESULTS AND IMPLEMENTATION DETAILS

### B.1 RESULTS

Mean Absolute errors for arithmetic tasks on integer sequences are reported in Table 4 and Table 5. These largely corroborate the results from Table 1, with a drop in the mean absolute error as the value of  $k$  increases and when using more sampled permutations at test-time (e.g., Janossy-20inf-LSTM versus Janossy-1inf-LSTM). Beyond the performance gains, we also observe a drop in variance when sampling more permutations at test time.

Table 6: Summary of the graph datasets

CHARACTERISTIC	CORA	PUBMED	PPI
Number of Vertices	2708	19717	56944, 2373 <sup>a</sup>
Average Degree	3.898	4.496	28.8 <sup>a</sup>
Number of Vertex Features	1433	500	50
Number of Classes	7	3	121 <sup>b</sup>
Number of Training Vertices	1208	18217	44906 <sup>c</sup>
Number of Test Vertices	1000	1000	5524 <sup>c</sup>

<sup>a</sup> The PPI dataset comprises several graphs, so the quantities marked with an “a”, represent the characteristic of the average graph .

<sup>b</sup> For PPI, there are 121 targets, each taking values in  $\{0, 1\}$ .

<sup>c</sup> All of the training nodes come from 20 graphs while the testing nodes come from two graphs not utilized during training.

## B.2 IMPLEMENTATION AND EXPERIMENT DETAILS

**Sequence tasks** We extended the code from Zaheer et al. (2017), which was written in Keras(Chollet et al., 2015), and subsequently ported to PyTorch. Regardless of the model, we always sort the sequence  $x$  beforehand. In the notation of Figure 1,  $h$  is an Embedding with dimension of  $\text{floor}(\frac{100}{k})$ ,  $\tilde{f}$  is either an MLP with a single hidden layer or an RNN depending on the model ( $k$ -ary Janossy or full-Janossy, respectively), and  $\rho$  is either a linear dense layer or one hidden layer followed by a linear dense layer. The MLPs in  $\tilde{f}$  have 30 neurons whereas the MLPs in  $\rho$  have 100 neurons, the LSTMs have 50 neurons, and the GRUs have 80 hidden neurons. All activations are tanh except for the output layer which is linear.

We constructed these models to be as comparable as possible; each has a similar number of total parameters and the same number of layers. We unify the number of parameters by adjusting the output dimension of the embedding (approximately  $\frac{1}{k}$ ) for the different  $k$ -ary models and by using fewer neurons in the LSTM than the GRU since LSTMs are more complicated models with more parameters.

Optimization is done with Adam (Kingma & Ba, 2015). We performed a sweep over the learning rate, with learning rate in  $[0.01, 0.001, 0.0001, 0.00001]$ . Training was performed on GeForce GTX 1080 Ti GPUs.

**Graph-based tasks** The datasets used for this task are summarized in Table 6. Our implementation is in PyTorch using Python 2.7, following the PyTorch code associated with Hamilton et al. (2017). That repo did not include an LSTM aggregator, so we implemented our own following the TensorFlow implementation of GraphSAGE, and describe it here. At the beginning of every forward pass, each vertex  $v$  is associated with a  $p$ -dimensional vertex attribute  $h$  (see Table6). For every vertex in a batch,  $k_1$  neighbors of  $v$  are sampled, their order is shuffled, and their features are fed through an LSTM. From the LSTM, we take the short-term hidden state associated with the last element in the input sequence (denoted  $h_{(T)}$  in the LSTM literature, but this  $h$  is not to be confused with a vertex attribute). This short-term hidden state is passed through a fully connected layer to yield a vector of dimension  $\frac{q}{2}$ , where  $q$  is a user-specified positive even integer referred to as the *embedding dimension*. The vertex’s own attribute  $h$  is also fed forward through a fully connected layer with  $\frac{q}{2}$  output neurons. At this point, for each vertex, we have two representation vectors of size  $\frac{q}{2}$  representing the vertex  $v$  and its neighbor set, which we concatenate to form an embedding of size  $q$ . This describes one convolution layer, and it is repeated a second time with a distinct set of learnable weights for the fully connected and LSTM layers, sampling  $k_2$  vertices from each neighborhood and using the embeddings of the first layer as features. After each convolution, we may optionally apply a ReLU activation and/or embedding normalization, and we follow the decisions shown in the GraphSAGE code Hamilton et al. (2017). After both convolution operations, we apply a final fully connected layer to obtain the score, followed by a softmax (Cora, Pubmed) or sigmoid (PPI). The loss function is cross entropy for Cora and Pubmed, and binary cross entropy for PPI.

Optimization is performed with the Adam optimizer (Kingma & Ba, 2015). The training routine for the smaller graphs (Cora, Pubmed) is not guaranteed to see the entire training data, in contrast with the scheme applied to the larger PPI graph. For Cora and Pubmed, we form 100 minibatches by

randomly sampling subsets of 256 vertices from the training dataset (with replacement). With PPI, we perform 10 full epochs: at each epoch, the training data is shuffled, partitioned into minibatches of size 512, and we pass over each. In either case, the weights are updated after computing the gradient of the loss on each minibatch.

The hyperparameters were set by following Hamilton et al. (2017); no hyperparameter optimization was performed. For every dataset, the embedding dimension was set to  $q = 256$  at both conv layers. For Pubmed and PPI, the learning rate is set at 0.01 while for Cora it is set at 0.005.

At test time, we load the weights obtained from training, perform 20 forward passes – which shuffles the input sequence by design – average the predicted probabilities (i.e. softmax output) from each forward pass, and choose the class that maximizes the averaged probabilities.

The implementation for Mean Pooling is similar in spirit but replaces  $\vec{f}$  with a permutation invariant function. The details can be found by viewing our repo on GitHub.